

Effect(s) of Cobalt Substitution in $L1_0$ -(Fe,Co)Pt Thin Films

Shoya Sakamoto,¹ Kumar Srinivasan,² Rui Zhang,^{2,*} Oleg Krupin,^{2,*}
Keisuke Ikeda,¹ Goro Shibata,¹ Yosuke Nonaka,¹ Zhendong Chi,¹ Masako
Sakamaki,³ Kenta Amemiya,³ Atsushi Fujimori,¹ and Antony Ajan²

¹*Department of Physics, The University of Tokyo,
7-3-1 Hongo, Bunkyo-ku, Tokyo 113-0033, Japan*

²*Western Digital Media, 1710 Automation Pkwy., San Jose, California 95131, USA*

³*Institute of Materials Structure Science,
High Energy Accelerator Research Organization,
1-1 Oho, Tsukuba, Ibaraki 305-0801, Japan*

(Dated: November 11, 2018)

Abstract

We have studied the effect of cobalt substitution in $L1_0$ -Fe_{1-x}Co_xPt films by means of x-ray magnetic circular dichroism (XMCD) and first-principles calculations. The magnetic moments of Fe ($\sim 2.5 \mu_B$) and Co ($\sim 1.5 \mu_B$) deduced using XMCD were almost unchanged upon Co doping, and the net magnetization decreases with increasing Co content. Calculation also showed that the $3d$ electrons that have been added by Co substitution occupy only spin-down bands.

Owing to the development of information technology, the amount of information has been increasing explosively. In such circumstances, hard disk drives (HDDs) have played a central role as storage devices, where the assembly of ferromagnetic grains is used as a bit. To achieve even higher areal bit density by decreasing the size of the grains, it is necessary to use materials with large magnetic anisotropy so that the decrease of the grain volume V is compensated by the increase of the magnetic anisotropy energy K , maintaining the thermal stabilization factor $KV/k_B T$ large enough, say above 60^1 . $L1_0$ -ordered FePt and CoPt are promising materials since they possess very large K of 7.0×10^7 erg/cc and 4.9×10^7 erg/cc, respectively^{2,3}. To utilize these materials as a media for HDDs, a large value of saturation magnetization M_S is also required to increase the signal level and to achieve an adequate signal to noise ratio (SNR). The reported M_S values of $L1_0$ FePt and CoPt are about 1100 emu/cc³⁻⁵ and 800 emu/cc^{3,6}, respectively, at room temperature.

In previous studies employing macroscopic magnetometry such as SQUID or vibrating sample magnetometer (VSM) measurements, mixed compounds $\text{Fe}_{1-x}\text{Co}_x\text{Pt}$ were reported to have larger net magnetization than pristine FePt, which would be a promising property for future HDD applications. A 14% increase was observed for $(\text{Fe}_{0.5}\text{Co}_{0.5})_{60.5}\text{Pt}_{39.5}$ bulk specimen⁷, 15% for $(\text{Fe}_{0.85}\text{Co}_{0.15})_{50}\text{Pt}_{50}$ thin film⁸, and even 54% for $(\text{Fe}_{0.8}\text{Co}_{0.2})_{59}\text{Pt}_{41}$ thin film⁹. However, first-principles calculations^{10,11} suggested that the net magnetization decreases with increasing Co content.

In order to resolve this issue, we have performed x-ray absorption spectroscopy (XAS) and x-ray magnetic circular dichroism (XMCD) measurements, by which one can obtain the (effective) spin and orbital magnetic moments of each constituent element separately¹²⁻¹⁴. Since XAS and XMCD are also sensitive to chemical states¹⁵, it is possible to deduce the intrinsic magnetic moments excluding contributions from impurities such as surface oxides^{16,17}. In addition, we have done first-principles calculations to deduce the magnetic dipole term in the spin sum rule and to discuss the effect of Co substitution in FePt films.

Samples were grown using the dc and rf sputtering methods on glass substrates. The sample structure was “C cap (4 nm)/ $\text{Fe}_{1-x}\text{Co}_x\text{Pt}$ (22 nm)/MgO (20 nm)/seed/glass substrate” ($x = 0, 0.05, 0.1, 0.15, 0.3$). Because we found strong oxide peaks in the XAS spectrum of the $x = 0$ sample, we used another sample with the different structure of “C cap (4 nm)/FePt (5 nm)/MgO (5 nm)/seed/glass substrate” for XAS and XMCD measurements. The MgO, C layers were grown at room temperature, while $\text{Fe}_{1-x}\text{Co}_x\text{Pt}$ layer was grown at the elevated temperature of 600 °C to

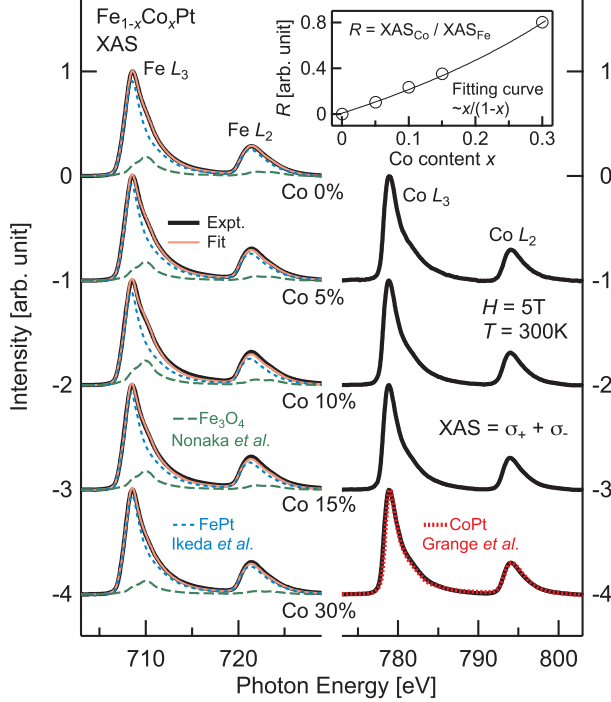


FIG. 1. Fe and Co $L_{2,3}$ -edge XAS spectra of $\text{Fe}_{1-x}\text{Co}_x\text{Pt}$. The Fe XAS spectra were fitted by the summation of FePt^{23} (blue dashed) and Fe_3O_4 (green dashed)²⁴ spectra. The fitted results are shown by pink solid curves. The XAS spectrum of $L1_0$ - CoPt^6 is also shown by a red dashed curve as a reference. The inset shows the ratio R of Co $L_{2,3}$ XAS integral to the Fe one as a function of Co content x .

achieve the (001)-oriented $L1_0$ -ordered phase¹⁸. We used separate Fe, Co and Pt targets to control the composition.

XAS and XMCD measurements were conducted at beam line BL-16A1 of Photon Factory (PF), High Energy Accelerator Research Organization (KEK). The spectra were taken at room temperature in the total-electron-yield (TEY) mode. A magnetic field of 5 T was applied parallel to the incident x rays and perpendicular to the film surface so that the magnetization of $\text{Fe}_{1-x}\text{Co}_x\text{Pt}$ was fully saturated. A double-step function with amplitude ratio 2:1 representing the L_3 - and L_2 -edge jumps has been subtracted from each absorption spectrum¹⁹.

First-principles calculations with the local-density approximation (LDA) were performed using a WIEN2k package. Spin-orbit interaction was also included. In order to study the effect of Co substitution, we constructed supercells containing Co atom at the Fe sites as shown in the supplemental material²⁰. We assumed Vegard's relation of $a = 3.863(1 - x) + 3.806x$ and $c = 3.710(1 - x) + 3.684x$ for the lattice constants of $\text{Fe}_{1-x}\text{Co}_x\text{Pt}^{21,22}$.

Figure 1 shows the XAS spectra of $\text{Fe}_{1-x}\text{Co}_x\text{Pt}$ recorded at the Fe and Co $L_{2,3}$ absorption edges, where they have been normalized to unity at the peak of the L_3 absorption edge for each element. The Fe XAS spectra show a shoulder around ~ 710 eV, which did not in the previous studies of FePt films^{23,25}. This can be attributed to signals from Fe oxides formed at the surface because the position of the shoulder corresponds to the peak position of the XAS spectra of Fe^{3+} compounds such as Fe_2O_3 ²⁵ and because the intensities of the shoulder showed non-monotonic behavior as a function of Co content. Such shoulders were not seen in the Co XAS spectra, where the spectral line shape did not change upon Co doping. This can be naturally understood because Co is more difficult to be oxidized than Fe. Since the Fe XAS spectra contain signals from surface oxides, we have decomposed the spectra into FePt²³ and Fe oxides components by least-square fitting. Here, we have used the Fe_3O_4 spectrum²⁴ in order to reflect the contributions from both Fe^{2+} and Fe^{3+} oxides. Note that the following discussion would not be affected if we adopt the Fe_2O_3 spectrum, but fit using the Fe_3O_4 better reproduced the experimental spectra as was also mentioned in Ref. 25. The fitted results are shown by pink solid curves, and the FePt and Fe_3O_4 spectrum components are also separately shown by blue and green dashed curves, respectively. This decomposition is crucial when estimating the magnetic moments using XMCD sum rules^{12,13}.

The inset of Fig. 1 shows the ratio of the XAS area of Co to that of Fe as a function of Co content x . The data are well fitted to $Ax/(1-x)$, where A is a proportionality constant. This confirms that the actual concentration of Fe and Co atoms, or at least its ratio, is very close to the designed values.

Figure 2 shows the XMCD spectra of $\text{Fe}_{1-x}\text{Co}_x\text{Pt}$. They are nearly identical to those of FePt²³ and CoPt⁶ as shown by blue and red dashed curves, respectively. This indicates that the local electronic structure of the $\text{Fe}_{1-x}\text{Co}_x\text{Pt}$ alloy is similar to their two end members FePt and CoPt. Note that the Fe-oxide shoulder seen in the XAS spectra was absent in the XMCD spectra, presumably because naturally formed Fe oxides are usually non-ferromagnetic.

We have estimated the spin and orbital magnetic moments of Fe and Co by applying the XMCD sum rules¹⁹:

$$m_l = -\frac{4 \int_{L_{2,3}} \sigma_+ - \sigma_- d\omega}{3 \int_{L_{2,3}} \sigma_+ + \sigma_- d\omega} n_h, \quad (1)$$

$$m_s^{\text{eff}} = -\frac{2 \int_{L_3} \sigma_+ - \sigma_- d\omega - 4 \int_{L_2} \sigma_+ - \sigma_- d\omega}{\int_{L_{2,3}} \sigma_+ + \sigma_- d\omega} n_h, \quad (2)$$

$$m_s^{\text{eff}} = m_s + 7m_T, \quad (3)$$

where σ_+ and σ_- denote absorption cross sections, namely XAS intensity, measured with x rays

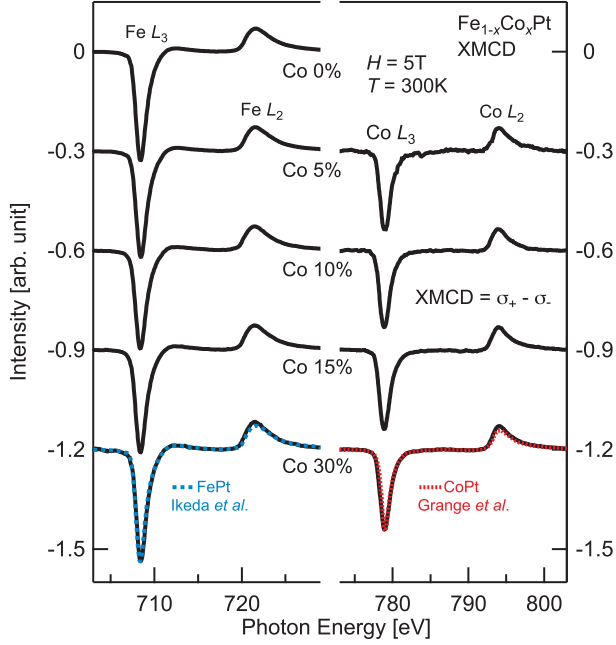


FIG. 2. XMCD spectra of $\text{Fe}_{1-x}\text{Co}_x\text{Pt}$ at Fe and Co $L_{2,3}$ edges. The spectra of $L1_0$ -ordered FePt and CoPt are shown as references by blue and red dashed curves, respectively.

with positive and negative helicity. m_l and m_s are the orbital and spin magnetic moments, m_s^{eff} the effective spin magnetic moment, and m_T the magnetic dipole term in units of μ_B/atom . Note that each term can be written as $m_s = -2\mu_B \langle S_\alpha \rangle / \hbar$, $m_l = -\mu_B \langle L_\alpha \rangle / \hbar$, and $m_T = -\mu_B \langle T_\alpha \rangle / \hbar$, where \mathbf{S} denotes the spin angular momentum operator, \mathbf{L} the orbital angular momentum operator \mathbf{T} the magnetic dipole operator $\mathbf{T} = \mathbf{S} - 3\hat{r}(\hat{r} \cdot \mathbf{S})$, and α represents the incident x-ray direction²⁶. The number of holes in the Fe and Co $3d$ shell, denoted by n_h , was assumed to be 3.4 and 2.63, respectively^{6,25}. As for the Fe XAS area, which appears in the denominators of Eqs. (1) and (2), we used the fitted FePt component to exclude oxide contributions. By applying this correction, the estimated magnetic moments increased by at most $\sim 30\%$.

Although m_T term can be ignored in cubic systems with T_d or O_h symmetry, it cannot be neglected in the case of highly anisotropic systems such as $L1_0$ -ordered alloys. Here we estimate the m_T of Fe (Co) atom in FePt (CoPt) as follows. When spin-orbit coupling is weak and charge and spin are decoupled as in $3d$ transition metals, m_T can be expressed as²⁶

$$7m_T \approx \sum_i \frac{7}{2} Q_\alpha^i m_s^i = \sum_i \frac{7}{2} Q_\alpha^i \Delta n_i \mu_B, \quad (4)$$

$$Q_\alpha^i = \langle d_i | Q_{\alpha\alpha} | d_i \rangle, Q_{\alpha\beta} = \delta_{\alpha\beta} - 3r_\alpha r_\beta / r^2, \quad (5)$$

TABLE I. Orbital and (effective) spin magnetic moments of Fe and Co in $\text{Fe}_{1-x}\text{Co}_x\text{Pt}$. m_l and m_s denote the orbital and spin magnetic moments, respectively, and $m_s^{\text{eff}} = m_s + 7m_T$ the effective spin magnetic moment, where m_T is the magnetic dipole term. m_{Fe} and m_{Co} represent the summation of the orbital and spin magnetic moments for each atom, where m_T term has been subtracted as described in the main text. $m_{\text{net}} (= (1-x)m_{\text{Fe}} + xm_{\text{Co}})$ represents the net magnetic moment, and M_{net} the net magnetization of the film in the units of emu/cc taking the Pt magnetic moments of $0.38(1-x) + 0.42x \mu_B$ into account. Note that uncertainties are shown in parentheses.

$\text{Fe}_{1-x}\text{Co}_x\text{Pt}$	Fe [μ_B]				Co [μ_B]				m_{net}	M_{net}
	m_l	$m_s + 7m_T$	m_l/m_s^{eff}	m_{Fe}	m_l	$m_s + 7m_T$	m_l/m_s^{eff}	m_{Co}	[μ_B]	[emu/cc]
$x = 0$	0.27(3)	2.07(10)	0.13(2)	2.49(11)	-	-	-	-	2.49(11)	961
0.05	0.25(3)	2.06(10)	0.12(1)	2.47(11)	0.22(4)	1.25(13)	0.17(3)	1.45(13)	2.42(10)	942
0.10	0.19(2)	2.04(10)	0.10(1)	2.39(10)	0.23(4)	1.12(12)	0.20(4)	1.33(11)	2.28(9)	896
0.15	0.20(2)	2.02(10)	0.10(1)	2.36(10)	0.22(4)	1.27(13)	0.17(3)	1.46(12)	2.23(9)	881
0.30	0.20(2)	2.12(11)	0.10(1)	2.45(11)	0.17(3)	1.31(14)	0.13(3)	1.47(12)	2.15(8)	863
0 (Expt. ²⁵)	0.19	2.21	0.09	2.40*	-	-	-	-	2.40*	931*
0 (LSDA)	0.072	2.87	-0.25	0.025	2.94	-	-	-	2.94	1110
1 (Expt. ⁶)	-	-	-	-	0.26	1.76	0.148	2.02*	2.02*	840*
1 (LSDA)	-	-	-	-	0.109	1.79	0.033	0.061	1.90	806
0-1 (CPA ¹⁰)	-	-	-	2.9	-	-	-	1.8	$2.9 - 1.1x$	

*Effective values containing $7m_T$ term.

where $\alpha, \beta = x, y, \text{ or } z$ denotes the Cartesian frame. m_s^i is the spin magnetic moment of electrons in a d_i orbital, which is directly related to $\Delta n_i (= n_{i,\uparrow} - n_{i,\downarrow})$ the difference between occupation numbers of spin-up and spin-down electrons in the orbital. The values of Q_α^i are summarized in Ref. 26, and Δn_i can be easily calculated by first-principles calculation. In the out-of-plane geometry, $7m_T$ of FePt and CoPt were calculated to be $-0.246 \mu_B$ and $0.0326 \mu_B$, respectively, while in the in-plane geometry, $0.123 \mu_B$ and $-0.0171 \mu_B$ ²⁷. These values agree with the sum rules applications to the calculated XMCD spectra by first-principles calculations²⁸. Therefore, one should be careful about the spin magnetic moment of Fe in FePt with high degree of $L1_0$ -order, where $m_s^{\text{eff}} = m_s + 7m_T$ may be smaller than m_s by at most $\sim 15\%$. Note that we could confirm

this simple calculation reproduced the reported values of m_T of CrO_2 ²⁹.

The obtained effective spin and orbital moments are summarized in TABLE I together with the previous experimental and theoretical results. The obtained spin magnetic moments of Fe are similar to the previous experimental study²⁵, but those of Co are smaller than the results of Ref. 6. This is probably because some of the Co atoms are magnetically inactive near the surface with oxidized Fe. In fact, if the area ratios of the raw Fe XAS spectra to the fitted FePt components are also multiplied to the Co magnetic moments, the values become as large as those in Ref. 6.

Figure 3(a) shows the magnetic moments $m_s + m_l$ of Fe taking the oxides component and m_T term into account. Although the raw data (black diamonds) showed non-monotonic behavior, the moments became almost constant after the subtraction of the oxides component from the raw XAS spectra as shown by orange squares. Further, the subtraction of the m_T term had a minor effect on how the magnetic moments behaves with Co content, as shown by blue circles. Here, the $7m_T$ term was most simply estimated as $(7m_T/m_s)^{\text{calc}}m_s^{\text{expt}}S$ by assuming a linear relationship between m_T and the degree of $L1_0$ order S . S was deduced from the intensity ratio of the superlattice peak $I(110)$ to the fundamental peak $I(200)$ in the in-plane XRD profiles³⁰ as $S^2 = \frac{(I(110)/I(200))^{\text{obs}}}{(I(110)/I(200))^{\text{theor}}}$ ³¹ and is plotted in Fig. 3(c). Note that the m_T term for Co is negligibly small according to our LDA calculation.

Figure 3(b) summarizes the corrected magnetic moments of Fe and Co and the net magnetic moments of $\text{Fe}_{1-x}\text{Co}_x\text{Pt}$. Since both the Fe and Co magnetic moments were almost constant as functions of Co content, the net magnetic moment was found to decrease with Co doping. This disagrees with the previous experiments⁷⁻⁹ but agrees with the theoretical prediction¹⁰. In Fig. 3(b), blue and red solid lines represent averaged values of the magnetic moment of Fe and Co, respectively, and green one values calculated from them. Fitting using a linear function also reproduced the blue and green lines, although fitting to the Co magnetic moment showed slightly increasing behavior due to the fewer data points. Note that the Pt magnetic moments, which can be as large as $0.38\text{-}0.42 \mu_B$ ²⁸, have not been considered.

Out-of-plane magnetic hysteresis curves were also measured by magneto-optical Kerr effect (MOKE) and are shown in Fig. 3(d). Coercive field (H_C) is also plotted in Fig. 3(c). In spite of the small change in the degree of $L1_0$ order caused by Co substitution, H_C or the magnetic anisotropy decreases rather rapidly.

In order to understand the microscopic mechanism why the magnetization decreased with Co doping, we have calculated the densities of states (DOSs) of $\text{Fe}_{1-x}\text{Co}_x\text{Pt}$. Fig. 4(a) shows the

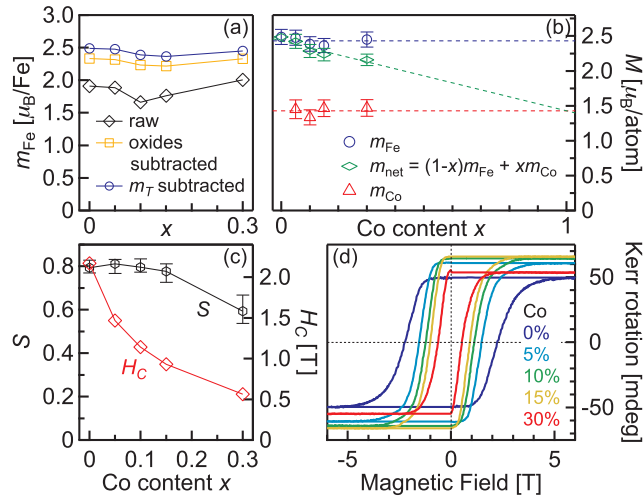


FIG. 3. (a) Magnetic moments of Fe before and after the corrections. (b) Magnetic moments of Fe and Co, and the net magnetic moment of $\text{Fe}_{1-x}\text{Co}_x\text{Pt}$ as a function of Co content. (c) Degree of $L1_0$ order and coercive field. (d) Out-of-plane magnetic hysteresis measured by magneto-optical Kerr effect.

Fe and Co partial DOS for varying the Co content. The DOSs of spin-up bands are almost fully occupied and unchanged upon doping, while those of spin-down bands shift upward without a significant change in the line shapes and concomitantly their occupation number increases. This suggests that the Co substitution does not change the band structure significantly, but simply provides the spin-down bands with electrons. The inset shows the electron occupation numbers of the spin-up and spin-down $3d$ bands (n_{3d}). The spin-up bands are almost completely filled with 4.5 electrons and the occupation number is nearly constant with Co content. On the other hand, the occupation number of the spin-down bands shows a linear increase. This can be understood because Co has one more $3d$ electron than Fe, and further electron doping leads to the occupation of spin-down bands. Note that the Pt partial DOS showed little change as shown in Fig. 4(b), and occupation number of Pt $5d$ orbitals was almost unchanged.

To summarize, the XMCD results have clarified that the net magnetic moment of $\text{Fe}_{1-x}\text{Co}_x\text{Pt}$ decreases with increasing Co content because the additional electron provided by Co occupy the spin-down bands instead of the almost completely filled spin-up bands. The discrepancy between the present results and the previous experiments⁷⁻⁹ would be attributed to some experimental artefacts such as errors in estimating the volume of FePt. Especially in the case of granular thin films, it is difficult to estimate the film thickness and the packing density of grains with sufficient accuracy. The present results also indicate that the magnetic moment may increase when holes

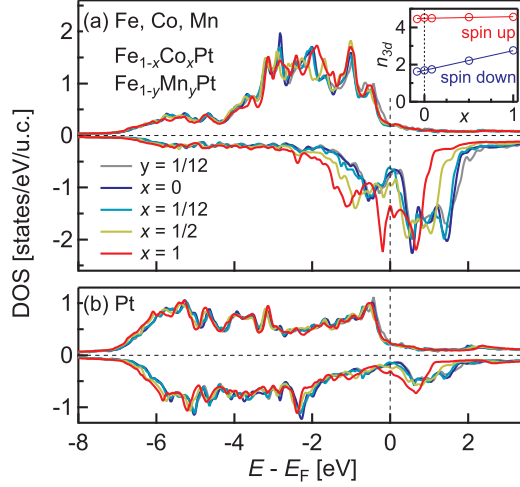


FIG. 4. Densities of states (DOSs) of $\text{Fe}_{1-x}\text{Co}_x\text{Pt}$ and $\text{Fe}_{1-y}\text{Mn}_y\text{Pt}$. The partial DOSs of the 3d transition metals and Pt are separately shown in panels (a) and (b). Inset shows the 3d orbital occupation number each of the spin-up and spin-down bands.

are doped to the system. To elaborate this conjecture, we have also calculated the DOS of Mn-substitute FePt. The spin-down DOS indeed shows a shift to the opposite direction, i.e., upward as expected. The occupation number is also plotted in the inset at the position of $x = -1/12$, representing a hole doping, and extrapolates from the trend of electron doping by Co. Therefore, the small amount of hole doping by Mn substitution or some other methods might be a better way to improve the magnetic properties of FePt. Actually, the effect of band filling^{32,33} and Mn substitution³⁴ to the magnetic properties of FePt were theoretically studied, and it was reported that the magnetic anisotropy as well as magnetization can be enhanced. However, too much doping may not be effective³⁵ because $L1_0$ -MnPt is antiferromagnetic.

This work was supported by Grants-in-Aid for Scientific Research from the JSPS (Grants No. 15H02109 and No. 15K17696). The experiment was done under the approval of the Photon Factory Program Advisory Committee (Proposals No. 2013S2-004, 2016S2-005 and No. 2016G006). S.S. acknowledges financial support from Advanced Leading Graduate Course for Photon Science (ALPS) and the JSPS Research Fellowship for Young Scientists. Z.C. acknowledges financial support from Materials Education program for the futures leaders in Research, Industry and Technology (MERIT). A.F. is an adjunct member of Center for Spintronics Research Network (CSRN),

the University of Tokyo, under Spintronics Research Network of Japan (Spin-RNJ).

* contributed during the stay at Western Digital

- ¹ S. H. Charap, P.-L. Lu, and Y. He, *IEEE Trans. Magn.* **33**, 978 (1997).
- ² M. Kryder, E. Gage, T. McDaniel, W. Challener, R. Rottmayer, G. Ju, Y.-T. Hsia, and M. Erden, *Proc. IEEE* **96**, 1810 (2008).
- ³ D. Weller, O. Mosendz, G. Parker, S. Pisana, and T. S. Santos, *Phys. Status Solidi A* **210**, 1245 (2013).
- ⁴ S. Okamoto, N. Kikuchi, O. Kitakami, T. Miyazaki, Y. Shimada, and K. Fukamichi, *Phys. Rev. B* **66**, 024413 (2002).
- ⁵ T. Bublath and D. Goll, *J. Appl. Phys.* **108**, 113910 (2010).
- ⁶ W. Grange, I. Galanakis, M. Alouani, M. Maret, J.-P. Kappler, and A. Rogalev, *Phys. Rev. B* **62**, 1157 (2000).
- ⁷ S. Saha, C. J. Thong, M. Q. Huang, R. T. Obermyer, B. J. Zande, V. K. Chandhok, S. Simizu, and S. G. Sankar, *J. Appl. Phys.* **91**, 8810 (2002).
- ⁸ Y. Liu and D. Sellmyer, *IEEE Trans. Magn.* **49**, 3292 (2013).
- ⁹ Y. Lai, Y. Chang, Y. Chen, H.-J. Lin, and G. Chen, *J. Mater. Sci.* **42**, 6887 (2007).
- ¹⁰ J. Maclaren, S. Willoughby, M. McHenry, B. Ramalingam, and S. Sankar, *IEEE Trans. Magn.* **37**, 1277 (2001).
- ¹¹ R. Cuadrado, T. J. Klemmer, and R. W. Chantrell, *Appl. Phys. Lett.* **105**, 152406 (2014).
- ¹² P. Carra, B. T. Thole, M. Altarelli, and X. Wang, *Phys. Rev. Lett.* **70**, 694 (1993).
- ¹³ B. T. Thole, P. Carra, F. Sette, and G. van der Laan, *Phys. Rev. Lett.* **68**, 1943 (1992).
- ¹⁴ J. Stöhr, *J. Electron. Spectrosc. Relat. Phenom.* **75**, 253 (1995).
- ¹⁵ F. de Groot, *J. Electron. Spectrosc. Relat. Phenom.* **67**, 529 (1994).
- ¹⁶ Y. Takeda, M. Kobayashi, T. Okane, T. Ohkochi, J. Okamoto, Y. Saitoh, K. Kobayashi, H. Yamagami, A. Fujimori, A. Tanaka, J. Okabayashi, M. Oshima, S. Ohya, P. N. Hai, and M. Tanaka, *Phys. Rev. Lett.* **100**, 247202 (2008).
- ¹⁷ S. Sakamoto, L. D. Anh, P. N. Hai, G. Shibata, Y. Takeda, M. Kobayashi, Y. Takahashi, T. Koide, M. Tanaka, and A. Fujimori, *Phys. Rev. B* **93**, 035203 (2016).
- ¹⁸ K. Barmak, J. Kim, L. H. Lewis, K. R. Coffey, M. F. Toney, A. J. Kellock, and J.-U. Thiele, *J. Appl.*

- Phys. **98**, 033904 (2005).
- ¹⁹ C. T. Chen, Y. U. Idzerda, H.-J. Lin, N. V. Smith, G. Meigs, E. Chaban, G. H. Ho, E. Pellegrin, and F. Sette, Phys. Rev. Lett. **75**, 152 (1995).
- ²⁰ See Supplemental Materials for further information.
- ²¹ K. Barmak, J. Kim, L. H. Lewis, K. R. Coffey, M. F. Toney, A. J. Kellock, and J.-U. Thiele, J. Appl. Phys. **95**, 7501 (2004).
- ²² I. Galanakis, M. Alouani, and H. Dreyssé, Phys. Rev. B **62**, 6475 (2000).
- ²³ K. Ikeda, T. Seki, G. Shibata, T. Kadono, K. Ishigami, Y. Takahashi, M. Horio, S. Sakamoto, Y. Nonaka, M. Sakamaki, K. Amemiya, N. Kawamura, M. Suzuki, K. Takanashi, and A. Fujimori, Appl. Phys. Lett. **111**, 142402 (2017).
- ²⁴ Y. Nonaka *et al.*, unpublished.
- ²⁵ O. Dmitrieva, M. Spasova, C. Antoniak, M. Acet, G. Dumpich, J. Kästner, M. Farle, K. Fauth, U. Wiedwald, H.-G. Boyen, and P. Ziemann, Phys. Rev. B **76**, 064414 (2007).
- ²⁶ J. Stöhr and H. König, Phys. Rev. Lett. **75**, 3748 (1995).
- ²⁷ In the out-of-plane geometry, where the direction of the light \vec{k} and the applied magnetic field \vec{H} are parallel to the z axis of the lattice or to the surface normal, $7m_T^z/\mu_B \approx -2\Delta n_{z^2} + 2\Delta n_{xy} + 2\Delta n_{x^2-y^2} - \Delta n_{yz} - \Delta n_{xz}$. In the in-plane geometry, where $\vec{k}, \vec{H} \parallel \vec{x}$, $7m_T^x/\mu_B \approx \Delta n_{z^2} - \Delta n_{xy} - \Delta n_{x^2-y^2} + 2\Delta n_{yz} - \Delta n_{xz}$ or just $m_T^x = -m_T^z/2$.
- ²⁸ I. Galanakis, M. Alouani, and H. Dreyssé, J. Magn. Magn. Mater. **242**, 27 (2002).
- ²⁹ M. Komelj, C. Ederer, and M. Fähnle, Phys. Rev. B **69**, 132409 (2004).
- ³⁰ Because the in-plane orientation of a and b axes are random in our granular films, one could directly compare the in-plane XRD intensity with simulated powder diffraction profile.
- ³¹ E. Yang, D. E. Laughlin, and J. G. Zhu, IEEE Trans. Magn. **48**, 7 (2012).
- ³² G. H. O. Daalderop, P. J. Kelly, and M. F. H. Schuurmans, Phys. Rev. B **44**, 12054 (1991).
- ³³ A. Sakuma, J. Phys. Soc. Jpn. **63**, 3053 (1994).
- ³⁴ T. Burkert, O. Eriksson, S. I. Simak, A. V. Ruban, B. Sanyal, L. Nordström, and J. M. Wills, Phys. Rev. B **71**, 134411 (2005).
- ³⁵ G. Meyer and J.-U. Thiele, Phys. Rev. B **73**, 214438 (2006).

Supplementary Information

SUPERCELLS

Figure 5 shows the supercells of $L1_0\text{-Fe}_{1-x}\text{Co}_x\text{Pt}$ ($x = 0, 1/12, 0.5, 1$) used in the present first-principles calculation. We assumed the smallest or simplest possible supercells with periodically located Co atoms for each Co concentration. For $x = 1/12$, two different supercells $2 \times 2 \times 3$ and $2 \times 3 \times 2$ are possible, but only the density of states (DOS) of the $2 \times 2 \times 3$ supercell is shown in the main manuscript. Note that we have confirmed the DOS of the $2 \times 3 \times 2$ was almost identical to that of $2 \times 2 \times 3$, indicating that the effect of Co doping is just an electron doping to the spin-down bands.

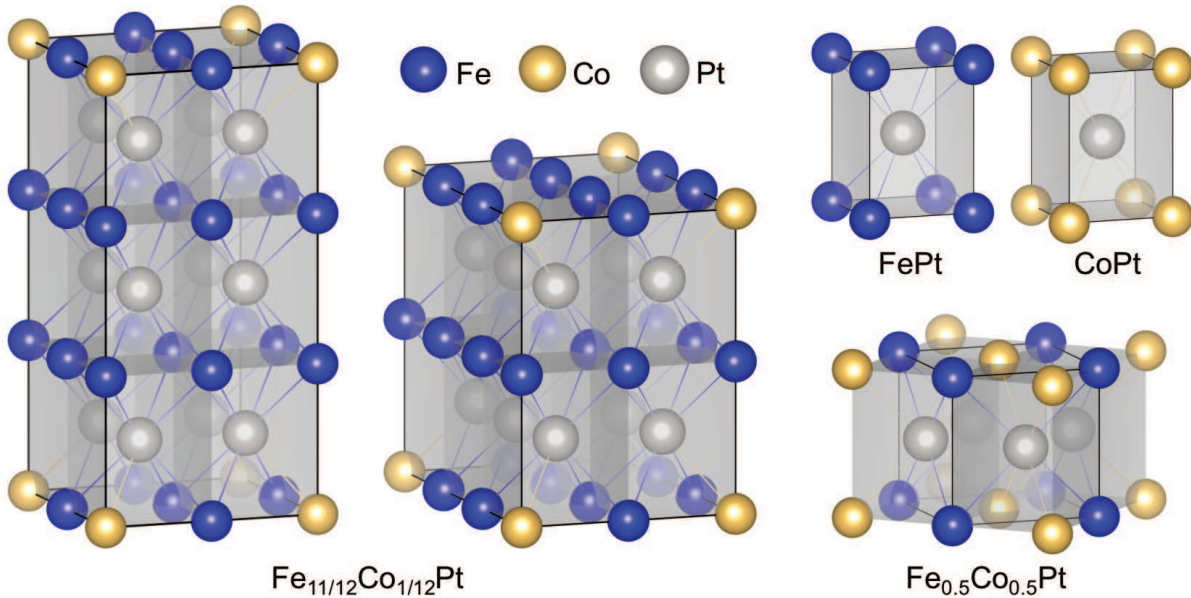


FIG. 5. Supercells of $\text{Fe}_{1-x}\text{Co}_x\text{Pt}$ ($x = 0, 1/12, 0.5, 1$) used in the first-principles calculations.